American Mineralogist, Volume 80, pages 1269–1276, 1995

# Stability and structure of a new high-pressure silicate, $Na_{1.8}Ca_{1.1}Si_6O_{14}$

TIBOR GASPARIK, JOHN B. PARISE
Center for High Pressure Research, Department of Earth and Space Sciences, State University of New York at Stony Brook, Stony Brook, New York 11794, U.S.A.
BONNIE A. EIBEN
Department of Geological Sciences, Rutgers University, New Brunswick, New Jersey 08903, U.S.A.
JOSEPH A. HRILJAC
Department of Applied Science, Brookhaven National Laboratory, Upton, New York 11973, U.S.A.

## ABSTRACT

Preliminary phase relations for the bulk composition $Na_2O \cdot CaO \cdot 5SiO_2$ were experimentally determined at 8–16 GPa and 950–2300 °C, using a split-sphere anvil apparatus (USSA-2000). The dominant phase at pressures between 8 and 14 GPa was a new compound with the ideal formula $Na_2CaSi_6O_{14}$; microprobe analyses suggest vacancies that cannot be resolved by X-ray data, resulting in a composition better expressed as $Na_{1.8}Ca_{1.1}Si_6O_{14}$. Single crystals suitable for structure determination were synthesized at 14 GPa and 1900 °C. Two independent sets of X-ray diffraction data were collected on different crystals from the same batch: one with a conventional diffractometer and the other using imaging plates and a synchrotron X-ray source. The compound crystallizes in space group $P321$ with $a = 7.903(2)$ and $c = 4.595(1)$ Å. Its structure consists of layers in (001); one is centered at $z = 0$ and contains the (Ca,Na) and $^{[6]}$Si sites. The other, centered at $z = ½$, is a sheet of corner-linked $^{[4]}$Si tetrahedra composed of open-branched crankshaft vierer chains linked by single tetrahedra. Although the $SiO_6$ octahedra are close to regular, with Si-O = 1.789(2) Å, the two symmetry-independent $SiO_4$ tetrahedra are distorted as a result of underbonding between O atoms bonding outside the sheet, with Si1-O = 1.557(2) and 1.638(2) Å, and Si2-O = 1.619(1) and 1.648(2) Å. Half-normal probability plots show the positional parameters derived from the two data sets to be statistically equivalent.

## INTRODUCTION

Ringwood and Major (1971) reported the synthesis of a new sodium garnet from a glass with the composition $Na_2CaSi_5O_{12}$ at 18 GPa and 1000 °C. The glass crystallized dominantly (>90%) to garnet with a lattice parameter 11.542 Å. However, its exact structure, composition, and $P$-$T$ stability range have not been determined. A Mg analog of this garnet, $Na_2MgSi_5O_{12}$, was found by Gasparik (1989) to be stable at pressures above 15 GPa. To verify the observations of Ringwood and Major (1971), preliminary phase relations were experimentally determined for the composition $Na_2O \cdot CaO \cdot 5SiO_2$. During these survey experiments, a new material with a composition close to $Na_{1.8}Ca_{1.1}Si_6O_{14}$ was discovered, and its stability and structure are reported here.

The products of high-pressure synthesis are often too fine grained for data collection using conventional single-crystal diffractometers. One alternative for small single crystals is the use of much brighter synchrotron X-ray sources. In the past, the use of serial detectors and a step-scanning mode with these sources was problematic for several reasons. These include beam movement owing to orbit instabilities and distortions in focusing optics caused by high heat loads, difficulties in accurately measuring the incident intensity actually illuminating a small crystal, and slow slewing between reflections caused by the need for very fine stepping motors to measure the sharp peaks accurately. The introduction of imaging-plate area detection combined with oscillation methods, where many peak intensities are measured simultaneously and frame overlap can be used to scale data (Bolotovsky, 1994; Bolotovsky et al., 1995), promises to alleviate these problems. The crystals we obtained of $Na_{1.8}Ca_{1.1}Si_6O_{14}$ were suitable for data collection using a serial diffractometer and a sealed X-ray tube. However, an opportunity arose to collect synchrotron data using a newly installed imaging-plate system on the X7B beamline at the nearby National Synchrotron Light Source (NSLS). The structure, discussed below, is sufficiently interesting and complex to allow meaningful statistical comparisons between the structural parameters derived using conventional and synchrotron X-ray sources. The higher sensitivity and resolution of the synchrotron data were also used to check for extra reflections indicative of potential ordering of Na and Ca within the structure.

0003–004X/95/1112–1269$02.00

**TABLE 1.** Experimental conditions and average compositions of phases obtained by electron microprobe

| Expt. | *t* (min) | *P** (GPa) | *T*** (°C) | Phase† | An.‡ | Composition (atoms) Na | Ca | Mg | Al | Si | O |
|---|---|---|---|---|---|---|---|---|---|---|---|
| 2196 | 6 | 8 | 1560 | L1 | 7 | 1.968 | 1.064 | 0.015 | 0.003 | 4.966 | 12 |
| | | | | N1 | 6 | 1.842 | 1.042 | 0.001 | 0.004 | 6.015 | 14 |
| 2164 | 6 | 10 | 1400 | | | | | | | | |
| 2174 | 8 | 10 | 1490 | | | | | | | | |
| 2176 | 6 | 10 | 1560 | | | | | | | | |
| 2183 | 6 | 10 | 1690 | L1 | 3 | 2.010 | 0.981 | 0.005 | 0.003 | 5.003 | 12 |
| | | | | L2 | 2 | 2.479 | 1.892 | 0.005 | 0.002 | 4.430 | 12 |
| | | | | N1 | 11 | 1.839 | 1.069 | 0.001 | 0.006 | 6.001 | 14 |
| 2162 | 6 | 12 | 1400 | | | | | | | | |
| 2182 | 4 | 12 | 1800 | L1 | 4 | 2.000 | 1.012 | 0.009 | 0.004 | 4.987 | 12 |
| | | | | L2 | 3 | 3.319 | 1.111 | 0.040 | 0.007 | 4.590 | 12 |
| | | | | N1 | 8 | 1.733 | 1.150 | 0.002 | 0.004 | 5.987 | 14 |
| 2249 | 120 | 14 | 1600 | N1 | 3 | 1.717 | 1.099 | 0 | 0.032 | 5.998 | 14 |
| 2187 | 5 | 14 | 1800 | L2 | 5 | 2.477 | 0.946 | 0 | 0.006 | 4.903 | 12 |
| | | | | NS | 2 | 1.655 | 0.277 | 0 | 0.021 | 4.432 | 10 |
| | | | | C1 | 3 | 0.020 | 0.975 | 0 | 0.002 | 2.006 | 5 |
| 2188 | 6 | 14 | 1900 | L1 | 3 | 1.868 | 0.989 | 0.019 | 0.026 | 5.009 | 12 |
| | | | | L2 | 2 | 3.760 | 0.598 | 0.229 | 0.016 | 4.635 | 12 |
| | | | | N1 | 8 | 1.773 | 1.051 | 0 | 0.003 | 6.029 | 14 |
| | | | | C1 | 1 | 0.017 | 0.953 | 0.006 | 0 | 2.016 | 5 |
| 2223 | 60 | 15 | 1780 | N1 | 2 | 1.866 | 1.078 | 0.008 | 0.003 | 5.988 | 14 |
| | | | | NS | 4 | 2.477 | 0.085 | 0.003 | 0.003 | 4.334 | 10 |
| | | | | C1 | 2 | 0.009 | 0.965 | 0.005 | 0.001 | 2.012 | 5 |
| 2197 | 6 | 15 | 1990 | N2 | 10 | 1.997 | 0.901 | 0.085 | 0.003 | 4.005 | 10 |
| 2208 | 6 | 15 | 2060 | L1 | 3 | 1.991 | 1.007 | 0.003 | 0.003 | 4.995 | 12 |
| | | | | L2 | 3 | 2.257 | 1.151 | 0.003 | 0.003 | 4.856 | 12 |
| | | | | N1 | 9 | 1.784 | 1.127 | 0.005 | 0.003 | 5.986 | 14 |
| | | | | NS | 1 | 1.962 | 0.245 | 0.016 | 0.005 | 4.375 | 10 |
| | | | | C1 | 2 | 0.007 | 1.001 | 0.001 | 0 | 1.997 | 5 |
| 2269 | 270 | 16 | 1100 | | | | | | | | |
| 2254 | 240 | 16 | 1340 | | | | | | | | |
| 2237 | 8 | 16 | 1600 | | | | | | | | |
| 2244 | 180 | 16 | 1600 | | | | | | | | |
| 2229 | 60 | 16 | 1800 | | | | | | | | |
| 2224 | 30 | 16 | 2050 | L2 | 3 | 2.990 | 0.919 | 0.197 | 0.005 | 4.691 | 12 |
| | | | | N1 | 3 | 1.675 | 1.133 | 0.002 | 0.016 | 6.002 | 14 |
| | | | | N2 | 21 | 2.078 | 0.785 | 0.165 | 0.005 | 4.002 | 10 |
| | | | | NS | 3 | 1.956 | 0.114 | 0.005 | 0.007 | 4.447 | 10 |
| | | | | C2 | 3 | 0.028 | 0.961 | 0.001 | 0.001 | 1.011 | 3 |
| 2217 | 4 | 16 | 2260 | L1 | 4 | 2.061 | 1.026 | 0.014 | 0.001 | 4.964 | 12 |
| | | | | L2 | 3 | 3.856 | 0.959 | 0.018 | 0 | 4.547 | 12 |
| | | | | N1 | 9 | 1.738 | 1.145 | 0.003 | 0.002 | 5.990 | 14 |
| | | | | C2 | 2 | 0.027 | 0.960 | 0.001 | 0 | 1.013 | 3 |

* Sample pressure, uncertainty ±0.3 GPa (Gasparik, 1989).

** Temperature at the center of the sample.

† Abbreviations: C1 = $CaSi_2O_5$, C2 = $CaSiO_3$ perovskite, L1 = superliquidus melt, L2 = partial melt, N1 = $Na_{1.8}Ca_{1.1}Si_6O_{14}$, N2 = $Na_2CaSi_4O_{10}$ (nonquenchable), NS = sodium silicate.

‡ The number of averaged analyses.

## EXPERIMENTAL TECHNIQUES

The 10 mm sample assembly described previously (Gasparik, 1989) was used for the phase-relations experiments and synthesis of single crystals in the USSA-2000 split-sphere anvil apparatus. The starting material was a mechanical mixture of high-purity $Na_2Si_2O_5$ (sodium disilicate), $CaSiO_3$ (synthetic wollastonite), and amorphous $SiO_2$. The samples were loaded into rhenium capsules and fired with the assembly under argon at 1000 °C for 1 h to assure anhydrous conditions. The assembly was compressed over several hours. Once the target pressure was reached, the temperature was then slowly increased, reaching the target value in 10–30 min. The duration of the experiments ranged from 4–8 min at the melting temperatures to 4.5 h at the lowest temperatures. Experiments were terminated by turning off the power, causing the sample temperature to drop to the temperature of the anvils (100–200 °C) within a second. The pressure was then slowly decreased to 1 bar over a period of several hours.

Temperature was measured with $W_3Re$ vs. $W_{25}Re$ thermocouples and controlled with a Eurotherm controller. Because of temperature gradients in the sample, each experiment provided information on phase relations in a 200 °C temperature interval. The samples were positioned in the assembly slightly off center, so that the hot spot was near one end of the samples, referred to as the hot end. The temperatures measured by the thermocouple were approximately the same as those in the center of the samples; the temperature increase from the center to the hot spot was about 50 °C, whereas the temperature decrease from the center to the cold end of the samples was approximately 150 °C. Details of the temperature

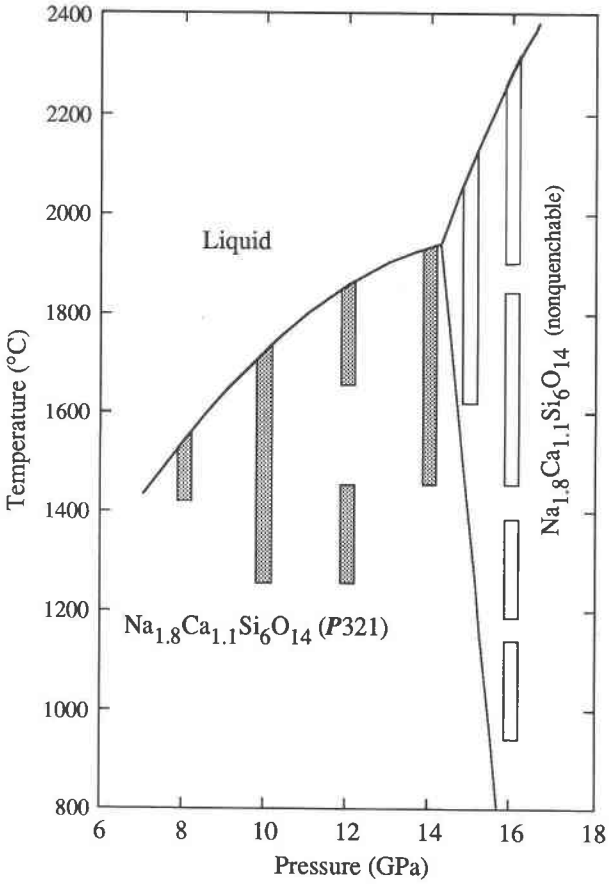


Fig. 1. Simplified temperature-pressure phase diagram for $Na_{1.8}Ca_{1.1}Si_6O_{14}$, based on the results of experiments with the composition $Na_2O \cdot CaO \cdot 5SiO_2$. Bars indicate the *P-T* location of the present experiments and the observed polymorph in the temperature interval corresponding to the subliquidus portion of the samples, assuming an interval of 200 °C in each sample.

Fig. 2. Backscattered electron image of the experimental product containing the crystals of $Na_{1.8}Ca_{1.1}Si_6O_{14}$ used for structure determination (Table 1, expt. 2188). The fine-grained material is a mixture of $CaSi_2O_5$ and sodium silicate. The scale bar is 100 $\mu$m long.

and pressure calibrations and experimental procedures were given by Gasparik (1989).

The samples, still inside the capsule, were mounted in epoxy. Polished mounts contained a lengthwise section of the samples, allowing inspection of phase relations along the full 200 °C interval. The experimental products were inspected visually under a microscope and analyzed for Na, Ca, Si, Mg, and Al with a Cameca electron microprobe. The time for counting simultaneously the first three elements (Na, Ca, and Si) was only 10 s, and a wider spot size was used whenever possible to minimize the Na loss. Close agreement between the analyses of the quenched glasses corresponding to superliquidus melts (L1 in Table 1) and the bulk composition of the starting material shows that the potential loss of Na during the analysis was negligible.

## Experimental results

The phase diagram based on the results of 20 experiments is shown in Figure 1, and the experimental conditions and observed compositions are summarized in Table 1. Because of the potential problems with metastability under subsolidus conditions, only the melting relations are reliable; a more definitive determination of the subsolidus phase relations would require the use of fluxes and reversals. However, the triple point at 1950 °C and 14.2 GPa is well located by the melting experiments. Melting was observed at 1550 °C and 8 GPa, 1730 °C and 10 GPa, 1850 °C and 12 GPa, 1940 °C and 14 GPa, 2110 °C and 15 GPa, and 2300 °C and 16 GPa. Melt quenched to transparent glass at 8–10 GPa and to crystals at higher pressures.

At pressures between 8 and 14 GPa, the dominant phase was a new compound with a composition close to $Na_2CaSi_6O_{14}$. However, the microprobe analyses consistently showed an excess of Ca (Table 1), apparently coupled with vacancies for charge balance, giving the average composition close to $Na_{1.8}Ca_{1.1}Si_6O_{14}$. The single crystals of this compound used for structure determination and refinement were synthesized at 14 GPa and 1900 °C (Table 1, expt. 2188) and were taken from the same mount that was used for the microprobe analysis (Fig. 2). At pressures above 14 GPa, the dominant phase had the same composition but became amorphous on quenching. The melting temperatures of this high-pressure polymorph increased rapidly with pressure, indicating a major gain in density relative to the low-pressure polymorph.

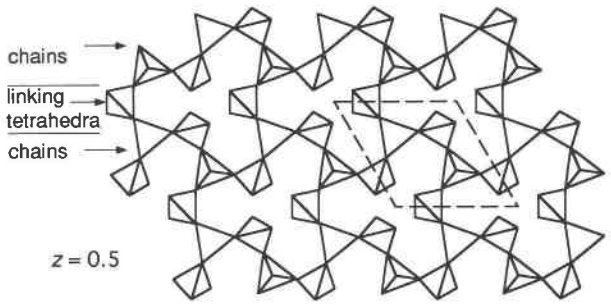


Fig. 3. The $(Si_5O_{14})^{8-}$ layer in $Na_{1.8}Ca_{1.1}Si_6O_{14}$ containing only Si tetrahedrally coordinated to O. These building units are corner linked to form open-branched crankshaft vierer chains (Liebau, 1985) crosslinked by tetrahedra to produce a novel sheet. These layers, at $z = ½$, are in (001) and alternate along [001] with Na-Ca-$^{[6]}$Si layers at $z = 0$ (Table 2).

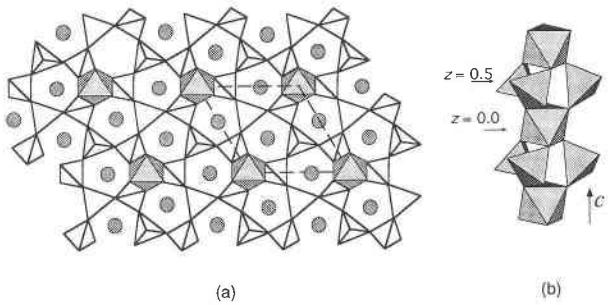


Fig. 4. (**a**) The Na-Ca-$^{[6]}$Si layer (shaded) superimposed over the tetrahedral layer (unshaded). Na and Ca are completely disordered in one site, Si is octahedrally coordinated to O in the other site. (**b**) The $^{[4]}$Si sheets are linked along the *c*-axial direction by $^{[6]}$Si octahedra.

The phase relations shown in Figure 1 are greatly simplified. The melting curve corresponds to the liquidus for the investigated bulk composition; several experiments at lower temperatures produced minor amounts of a Na-rich melt. Other Na- and Ca-bearing phases with lower silica contents coexisted with both polymorphs, as well as sodium silicate, stishovite, and either $CaSi_2O_5$ at 14–15 GPa or $CaSiO_3$ perovskite at 16 GPa (Table 1). The experimental products obtained at 16 GPa and subsolidus temperatures consisted of $Na_{1.8}Ca_{1.1}Si_6O_{14}$, $CaSiO_3$ perovskite, and sodium silicate and were found by X-rays to be amorphous after quenching.

## Diffraction measurements

Precession and Weissenberg X-ray photographs, used to identify crystals suitable for structure determination, were consistent with Laue symmetry $\bar{3}m1$. Data were collected from a clear, colorless single crystal (100 × 50 × 80 μm) at 295 K on a Picker diffractometer equipped with a graphite monochromator and using Mo$K\alpha$ radiation. Unit-cell parameters were determined to be $a = 7.903(2)$ and $c = 4.595(1)$ Å from 24 reflections in the range $20° < 2\theta < 29°$. A total of 1989 intensities were measured to $2\theta = 65°$ for $-11 < h < 11$, $0 < k < 11$, $-8 < l < 8$; a standard reflection was monitored every 20 reflections and showed no systematic variation over the course of the data collection. Data were corrected for Lorentz and polarization but not for absorption ($\mu = 15.7$ cm$^{-1}$) effects. Inspection of the intensity distribution confirmed the possible space groups as $P321$, $P3m1$, and $P\bar{3}m1$. A subsequent survey of the structure models derived from direct methods suggested $P321$ as the correct space group. The data were merged accordingly ($R_{merge} = 1.20\%$) to yield 573 unique data with $F > 3\sigma(F)$.

Structure solution and refinement were performed using values of F and statistical weights from a software package written and maintained by Calabrese (1994). A direct-method (Sheldrick, 1986) solution revealed the structure of the silicate layer (Fig. 3), and subsequent Fourier-difference maps indicated the positions of the remaining sites (Fig. 4). Only one position was found for Na and Ca in the structure, indicating disorder in this site. Neither long-exposure precession photographs nor the subsequent data collection using imaging plates indicated the presence of a superstructure. The scattering factor for the Na-Ca site was made consistent with the microprobe analysis ($Na_{0.600}Ca_{0.367}$). Full-matrix least-squares refinement converged to the results given in Table 2. The coordinates for the final model were inverted and refined to confirm the correct enantiomorph.

The desire to check for extra reflections indicative of possible ordering of Na and Ca within the structure, as well as some unusual atomic parameters and interatomic distances, prompted us to seek the confirmation of the refined model by collecting higher resolution data with imaging plates. The unusual features include the relatively short distance between Si1 and O2 in the $SiO_4$ tetrahedron, the comparatively large and anisotropic atomic displacement parameters for O1 and O2, and the large O3-Si2-O3 angle (Tables 2 and 3; Fig. 5).

An independent set of data was collected on a crystal from the same batch (60 × 60 × 60 μm) using imaging plates on the X7B beamline at the NSLS. The crystal was mounted on a goniometer head and placed on a Huber four-circle diffractometer at ambient temperature. A wavelength of 0.8892 Å was obtained using the following optical elements: a rhodium-plated spherical mirror; a fixed-exit, double-crystal Si(111) monochromator; and a rhodium-plated, bent toroidal focusing mirror. The beam shape was defined with a 500 μm pinhole collimator. Prior to the imaging-plate work, an accurate orientation matrix and unit cell were obtained by a least-squares refinement using the angular positions of 60 well-centered reflections measured in a standard step-scanning mode, giving $a = 7.899$ and $c = 4.595$ Å. An imaging-plate cassette holder was mounted on the detector arm and replaced the scintillation counter. This allowed a variable crystal-to-plate distance and a $2\theta$ offset angle. For this study, the sample-to-plate distance was set at 98 mm, and full data sets were collected at both $2\theta = 0$ and 45°, limiting the maximum scattering vectors to 1.02 and 0.59

**TABLE 2.** Fractional atomic coordinates and equivalent isotropic displacement parameters (Å²) for $Na_{1.8}Ca_{1.1}Si_6O_{14}$

| Atom | Multiplicity | Site sym.* | *x* | *y* | *z* | $B_{eq}$ |
|---|---|---|---|---|---|---|
| Si1 | 2 | 3.. | ⅔ | ⅓ | 0.4899(1) | 0.4 |
| | | | ⅔ | ⅓ | 0.4901(1) | 0.3 |
| Si2 | 3 | .2. | 0.74751(6) | *x* | ½ | 0.4 |
| | | | 0.74762(6) | *x* | ½ | 0.3 |
| Si3 | 1 | 32. | 0 | 0 | 0 | 0.4 |
| | | | 0 | 0 | 0 | 0.3 |
| Na/Ca1 | 3 | .2. | 0.41485(8) | *x* | 0 | 0.9 |
| | | | 0.41495(8) | *x* | 0 | 0.7 |
| O1 | 6 | 1 | 0.7021(2) | 0.5394(1) | 0.3505(2) | 0.8 |
| | | | 0.7018(2) | 0.5393(2) | 0.3504(2) | 0.8 |
| O2 | 2 | 3.. | ⅔ | ⅓ | 0.8288(4) | 1.2 |
| | | | ⅔ | ⅓ | 0.8295(4) | 1.2 |
| O3 | 6 | 1 | 0.8963(2) | 0.7899(1) | 0.7684(2) | 0.5 |
| | | | 0.8961(2) | 0.7899(1) | 0.7679(2) | 0.4 |

*Note:* $B_{eq} = (8\pi^2/3)\Sigma_i\Sigma_j U_{ij} a_i^* a_j^* \mathbf{a}_i \cdot \mathbf{a}_j$. Data collected on a diffractometer (first line) and with imaging plates (second line).

* Space group *P*321 (no. 150), for both data sets $w = [s^2(I) + 0.0009 \cdot I^2]^{-1/2}$, 37 parameters refined, discrepancy factors defined as $R = \Sigma (|F_o| - |F_c|)/S|F_o|$; $R_w = [\Sigma w(|F_o| - |F_c|)^2/Sw|F_o|^2]^{1/2}$; *R*, $R_w$, GOF, $\Delta/\sigma_{max}$, and data/parameter ratios are 1.92, 2.07, 1.05, <0.004, and 15.5, for Picker data, and 2.82, 2.87, 1.13, <0.004, and 27.1 for synchroton data.

**TABLE 3.** Anisotropic displacement parameters (× 10³ Å²) for $Na_{1.8}Ca_{1.1}Si_6O_{14}$

| Atom | $U_{11}$ | $U_{22}$ | $U_{33}$ | $U_{12}$ | $U_{13}$ | $U_{23}$ |
|---|---|---|---|---|---|---|
| Si1 | 5.5(2) | $U_{11}$ | 5.6(2) | ½$U_{11}$ | 0 | 0 |
| | 3.9(1) | $U_{11}$ | 4.8(2) | ½$U_{11}$ | 0 | 0 |
| Si2 | 5.0(2) | $U_{11}$ | 4.0(2) | 2.5(2) | −0.3(1) | $U_{13}$ |
| | 3.1(1) | $U_{11}$ | 3.2(1) | 1.3(1) | −0.2(1) | $U_{13}$ |
| Si3 | 5.4(2) | $U_{11}$ | 3.3(3) | ½$U_{11}$ | 0 | 0 |
| | 3.4(2) | $U_{11}$ | 2.7(2) | ½$U_{11}$ | 0 | 0 |
| Na/Ca1 | 10.7(2) | $U_{11}$ | 9.3(2) | 4.0(2) | 0.5(1) | $U_{13}$ |
| | 8.3(1) | $U_{11}$ | 8.8(2) | 2.8(2) | 0.5(1) | $U_{13}$ |
| O1 | 17.8(5) | 6.7(4) | 8.1(4) | 6.5(4) | −2.7(4) | −1.1(3) |
| | 16.4(4) | 4.9(3) | 7.7(3) | 5.4(3) | −3.4(3) | −0.7(3) |
| O2 | 20.6(6) | $U_{11}$ | 5.9(6) | ½$U_{11}$ | 0 | 0 |
| | 19.4(5) | $U_{11}$ | 5.3(5) | ½$U_{11}$ | 0 | 0 |
| O3 | 7.3(4) | 6.9(4) | 5.3(3) | 3.9(4) | −2.1(3) | −1.1(2) |
| | 5.3(3) | 4.9(3) | 4.7(2) | 2.3(3) | −1.7(2) | −1.1(2) |

*Note:* $\text{Exp}\{2\pi^2[U_{11}hha^*a^* \cdots + 2(U_{12}hka^*b^* \cdots)]\}$. Data collected on a diffractometer (first line) and with imaging plates (second line).

Å⁻¹, respectively. During the data collection, the crystal was rotated by 20° about $\phi$ during each of the 26.7 s exposures and then moved back 5° prior to the next scan. Twelve exposures were collected at each $2\theta$ setting covering a $\phi$ range of 185°. The Fuji Type III plates were read using a BAS-2000 scanner with a $10^4$ dynamic range.

The images were first processed with the program IPMS (Bolotovsky, 1994), which searches for peaks, indexes them on the basis of the known orientation matrix, and then refines the geometrical factors, including the crystal-to-plate distance and the imaging-plate tilt angles. Each scan contained between 140 and 195 peaks, which had a peak-to-background ratio greater than ten and were indexed on the basis of the unit cell used to collect data at Stony Brook. There was no indication of a superstructure. The final integration of the peak intensities was performed with the program HIPPO using the seed-skewness method (Bolotovsky et al., 1995), and this was followed by Lorentz and polarization corrections. Only fully recorded reflections were used; those close to the oscillation axis and boundaries were discarded. Using the program SORTAV (Blessing, 1989), 4080 reflections were scaled, sorted, and merged in point group 3 ($R_{merge}$ = 3.83%) to yield 1361 data. These were merged in point group 32 ($R_{merge}$ = 1.37%) using the program Z (Calabrese, 1994) to yield 1006 unique data with $F > 3\sigma(F)$.

Full-matrix least-squares refinement, using the parameters derived from the Picker data set as a starting point, converged to the results given in Table 2. An attempt was made to refine the occupancy of the Na-Ca site using a composite scattering factor for the composition derived from the microprobe analyses, $Na_{0.600}Ca_{0.367}$. As expected, the results of full least-squares refinement were inconclusive, with typical refined occupancies of 1.013(5), many correlation matrix elements > 0.75 between thermal and occupancy parameters, and slow convergence. Similar results were obtained for the Picker data, although the typical value of the refined occupancy factor for the Na-Ca site was 0.995(4). The results of the microprobe analysis were used to constrain the site composition and occupancy for the final refinement (Tables 2 and 3).

## DISCUSSION

### The structure

The compound $Na_{1.8}Ca_{1.1}Si_6O_{14}$ represents another of a growing number of examples of high-pressure phases

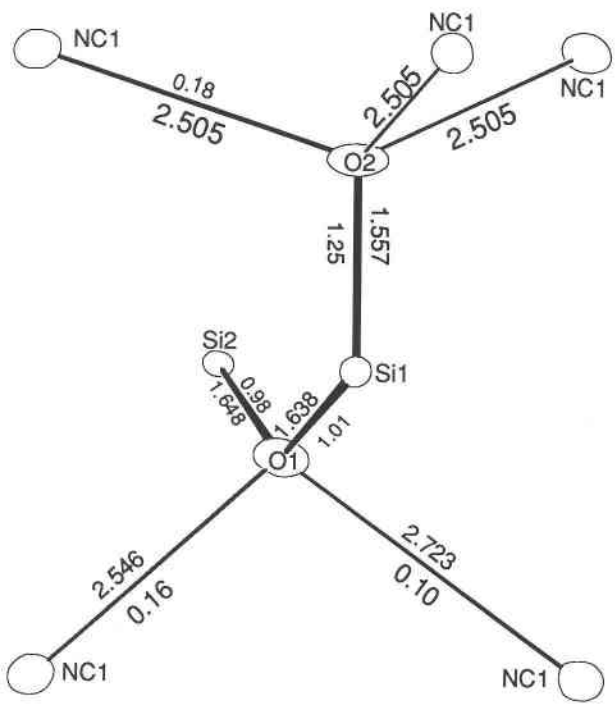


Fig. 5. Representation of the coordination environment about O1 and O2 using the thermal ellipsoid plot program, ORTEP (Johnson, 1976). The label NC refers to sites partially occupied by Na and Ca ($Na_{0.600}Ca_{0.367}$). Interatomic distances (Å) and the corresponding bond valences (Brown, 1981; Brown and Shannon, 1973) are indicated.

**TABLE 4.** Selected interatomic distances (Å) and angles (°) for $Na_{1.8}Ca_{1.1}Si_6O_{14}$ derived from data collected on a diffractometer

| Atoms* | Dist/ang. | Atoms* | Dist/ang. |
|---|---|---|---|
| Si1-O1 × 3 | 1.638(2) | NC1-O3$^f$ × 2 | 2.398(2) |
| Si1-O2 | 1.557(2) | | |
| Si2-O1 × 2 | 1.648(2) | O1-NC1-O1$^g$ | 100.55(7) |
| Si2-O3 × 2 | 1.619(1) | O1$^a$-NC1-O2$^e$ | 65.45(5) |
| Si3-O3 × 6 | 1.789(2) | O1$^a$-NC1-O2$^a$ | 125.20(7) |
| | | O1-NC1-O2$^e$ | 91.60(6) |
| O1-Si1-O1 × 2 | 105.72(7) | O1-NC1-O2$^e$ | 68.20(8) |
| O1-Si1-O2 | 113.00(4) | O1$^a$-NC1-O3$^f$ | 77.74(8) |
| O1-Si2-O1$^a$ | 105.13(9) | O1-NC1-O3$^f$ | 133.77(4) |
| O1-Si2-O3$^a$ | 105.67(8) | O1-NC1-O3$^h$ | 112.91(7) |
| O1-Si2-O3 | 107.28(5) | O1$^a$-NC1-O3$^h$ | 72.89(7) |
| O3-Si2-O3$^a$ | 124.39(8) | O2$^e$-NC1-O2$^e$ | 148.84(3) |
| O3-Si3-O3$^b$ | 92.23(8) | O2$^e$-NC1-O3$^h$ | 129.51(7) |
| O3-Si3-O3 × 3 | 179.3(2) | O2$^e$-NC1-O3$^f$ | 79.52(7) |
| O3-Si3-O3$^c$ | 88.23(6) | O3$^f$-NC1-O3$^h$ | 64.49(6) |
| O3-Si3-O3$^d$ | 91.3(1) | O1-NC1-O1$^a$ | 59.32(6) |
| | | O1$^a$-NC1-O1$^i$ | 145.15(5) |
| NC1-O1 × 2 | 2.546(2) | O1-NC1-O1$^i$ | 153.26(4) |
| NC1-O1$^a$ × 2 | 2.723(2) | | |
| NC1-O2$^e$ × 2 | 2.505(2) | | |

*Note:* Symmetry operation codes: a = $y, x, 1 - z$; b = $y, x, 2 - z$; c = $2 - y, 1 + x - y, z$; d = $2 - x, 1 + y - x, 2 - z$; e = $x, y, -1 + z$; f = $1 - y, x - y, -1 + z$; g = $y, x, -z$; h = $x - y, 1 - y, 1 - z$; and i = $x - y, 1 - y, -z$.

* NC represents the Na-Ca site with composition ($Na_{0.600}Ca_{0.367}$).

containing Si in both four ($^{[4]}$Si) and six ($^{[6]}$Si) coordination with O (Swanson and Prewitt, 1983; Angel et al., 1988; Finger et al., 1989; Pacalo and Parise, 1992; Hazen et al., 1994). The framework of $Na_{1.8}Ca_{1.1}Si_6O_{14}$, shown in Figures 3 and 4, is composed of the ordered intergrowth of two structural elements. One of these is a layer in (001) consisting of corner-linked $SiO_4$ tetrahedra (Fig. 3) at $z = ½$ (Table 2). It consists of open-branched crankshaft vierer chains (Liebau, 1985) crosslinked by individual tetrahedra. The linkage occurs every second tetrahedron along the chain to produce a novel anionic sheet. This sheet contains two types of coordination environments for the $Si^{4+}$ and $Na^+$-$Ca^{2+}$ cations above and below it, at $z = 1.0$ and 0.0, which constitute the second structural element (Fig. 4). As in most other structures containing both $^{[4]}$Si and $^{[6]}$Si, the tetrahedrally and octahedrally coordinated Si atoms are partitioned into different structural elements. The $^{[6]}Si^{4+}$ (Si3 in Table 2) is located at the origin of the unit cell (Figs. 3 and 4), coordinated by three O atoms from each of the $(^{[4]}Si_5O_{14})^{8-}$ sheets above and below it.

The coordination about Si3 is close to a regular octahedron. On the other hand, the coordination about Si1 and Si2 is significantly distorted from tetrahedral (Table 3), with unusual interatomic distances and displacement parameters involving O2 and O3. Analysis of the bond-valence contributions (Brown and Shannon, 1973; Brown, 1981) suggests that the origin of the short Si1-O2 distance lies in the underbonding of this O with respect to the other O atoms in the structure. The valence sums about O1, O2, and O3 are 2.25, 1.79, and 1.96, respectively (Fig. 5), consistent with the larger atomic displacement parameter for O2 and the shorter than expected Si-O distance for this bond (Tables 3 and 4; Fig. 5). The shape of the anisotropic displacement ellipsoids for O1 and O2 may be a response to either the disorder in the Na-Ca site or to the uneven distribution of bond strengths about the O atoms (Fig. 5).

### Comparison of parameters from the two refinements

The crystal-chemical arguments made in the previous section are predicated on the positional and displacement parameters, derived from the single-crystal investigations, being representative of the bulk material (Tables 2 and 3). A demonstration of the statistical equivalence of the two sets of derived parameters would tend to validate this assumption. Several statistical tests can be used to analyze structural models for the evidence of a systematic bias. However, simple inspection of Table 2 suggests that the two sets of parameters are equivalent. Similarly, inspection of Table 3 suggests that the relative magnitude and orientation of the displacement parameters are comparable, but that the parameters derived from the data set collected at the synchrotron are underestimated in comparison with the data collected with a conventional diffractometer. Abrahams and Keve (1971) showed that half-normal probability plot analysis can be applied to parameters derived from two independent sets of measurements. Differences between pairs of positional and displacement parameters ($\Delta p$) can be examined in terms of their pooled standard deviations ($\sigma p$) by plotting the ordered statistic, $\delta p = \Delta p/\sigma p$, against the expected normal distribution. For correctly assigned standard deviations and a normal error distribution between experiment and model, a half-normal probability plot is linear with a unit slope and zero intercept. Deviations from linearity indicate some systematic differences between the parameter sets. Large differences between individuals in a pair of parameters ($\Delta p/\sigma p$) are seen at the extremity of the plot.

Figure 6a and 6b are half-normal probability plots for the positional and anisotropic displacement parameters derived from data for two different crystals of $Na_{1.8}Ca_{1.1}Si_6O_{14}$. The distribution of points (about a straight line of unit slope passing through the origin) for the pairs of positional parameters in Figure 6a shows that (1) there is no systematic bias between the two data sets, (2) the pooled standard deviations are correctly estimated, and (3) because the line passes through zero there is no systematic error between the two sets of parameters. The ordered array of real $\delta p$, shown in Figure 6b for anisotropic displacement parameters, points at zero but has a slope of about 4, indicating that either the $\Delta p$ are too large, the $\sigma p$ too small, or that both conditions are applicable. The near linearity and zero intercept of the plot suggest that the major contribution to the nonunit slope is the underestimation of the standard deviations (Abrahams and Keve, 1971).

Apart from confirming the structural model, including the relative magnitudes of the displacement parameters, this analysis suggests that the data obtained with the synchrotron using imaging plates give results consistent with

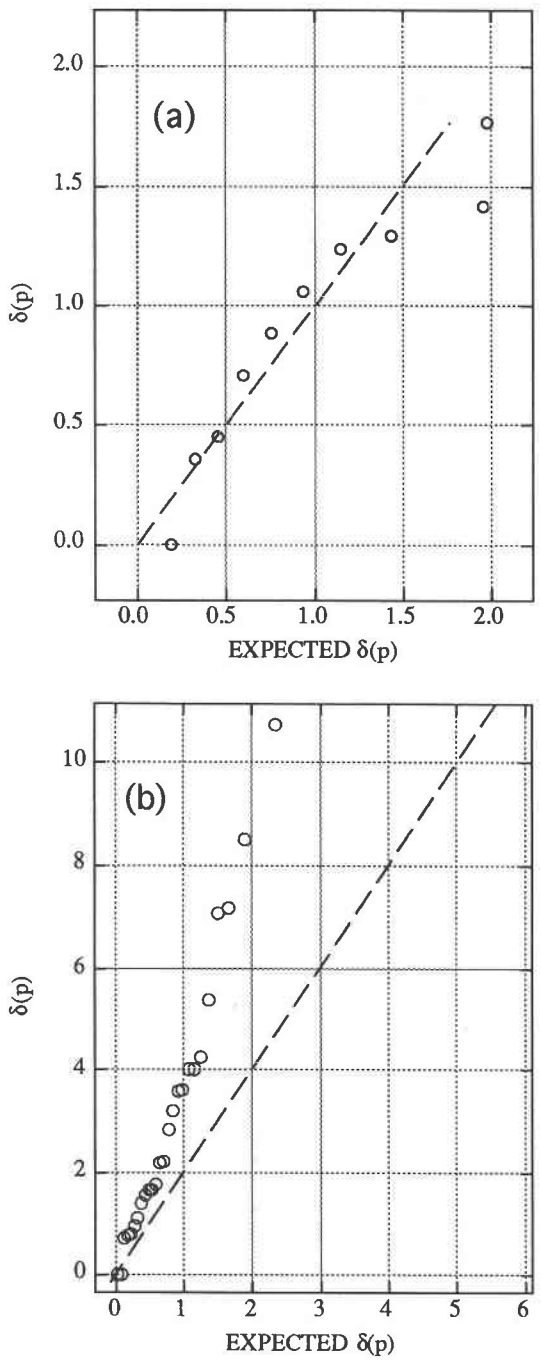


Fig. 6. Half-normal probability plots (Abrahams and Keve, 1971) for the refined positional (**a**) and anisotropic (**b**) parameters of $Na_{1.8}Ca_{1.1}Si_6O_{14}$ obtained with a diffractometer and the imaging plates. (**a**) For positional parameters, the normal distribution of errors indicates that the two sets of parameters belong to the same statistical family and are indistinguishable. The dashed line indicates the unit slope. (**b**) For anisotropic displacement parameters, the nonunit slope of the plot indicates underestimated standard deviations. The dashed line has the slope of 2.

those obtained by traditional diffraction techniques. It is important to point out that the total exposure time to the crystal during data collection with the imaging plates was about 11 min, although the real time for collecting the 24 patterns was 5 h because of the time required to read the plates. This suggests that even with much finer grained materials, more common in high-pressure synthesis, it is possible to obtain high-quality single-crystal data rapidly using the strategies outlined here.

### The structure of the high-pressure polymorph

The high-pressure polymorph of $Na_{1.8}Ca_{1.1}Si_6O_{14}$, stable at pressures > 14 GPa, is nonquenchable; hence, its structure can only be determined in situ. However, it is possible to make some predictions on the basis of the melting relations, the composition, and the structure of the low-pressure polymorph.

The deep cusp in the melting curve shown in Figure 1 is similar to the cusp observed in the $CaSiO_3$ system, the latter of which is due primarily to the formation of $CaSiO_3$ perovskite (Gasparik et al., 1994). The corresponding sharp increase in the melting temperatures with pressure reflects a major increase in densities, which, in the case of $CaSiO_3$ perovskite, is caused by the change in the coordination of Si to fully octahedral. Thus, it is plausible that the high-pressure polymorph of $Na_{1.8}Ca_{1.1}Si_6O_{14}$ also has all Si in the octahedral coordination.

Microprobe analyses show that the high-pressure polymorph is compositionally identical to the low-pressure polymorph, including the nonstoichiometry caused by vacancies. In the low-pressure polymorph, the composition, with its subtle nonstoichiometry, is determined by the structural properties of the Na-Ca-$^{[6]}$Si layer and is not expected to reproduce exactly in a different structural environment. Hence, the high-pressure polymorph may have a similar Na-Ca-$^{[6]}$Si layer. In this case, the structural difference would be in the silica layer; presumably, the $^{[4]}$Si layer is replaced in the high-pressure polymorph by a $^{[6]}$Si layer.

The high-pressure experiments failed to confirm the reported stability of $Na_2CaSi_5O_{12}$ garnet. Because the Si in this garnet is in a mixed coordination and its structure is quenchable, the stability field of garnet is not likely to be located at pressures higher than the observed stability of the high-pressure polymorph of $Na_{1.8}Ca_{1.1}Si_6O_{14}$. The rate of equilibration was found to be very slow under subsolidus temperatures, thus the garnet observed by Ringwood and Major (1971) may have formed metastably. Inadvertent contamination of the starting material would also stabilize garnet.

## Acknowledgments

We are grateful to Robert Bolotovsky (SUNY at Buffalo), Jon Hanson (NSLS), and Martin Kunz (SUNY at Stony Brook) for their help with the data collection at X7B and the subsequent analysis. This work was supported by the National Science Foundation (NSF) grants EAR-9303865 (to T.G.) and DMR-9413003 (to J.B.P.). B.A.E. was supported by the NSF grant EAR-9322426 for undergraduate research (to D.J. Weidner). The high-pressure experiments reported in this paper were performed in

the Stony Brook High Pressure Laboratory, which is jointly supported by the NSF Science and Technology Center for High Pressure Research (EAR-8920239) and SUNY at Stony Brook. Research performed at the National Synchrotron Light Source is supported by the U.S. Department of Energy, Basic Energy Sciences Division, Divisions of Materials Science and Chemical Sciences, Contract DE-AC02-76CH00016.

## References cited

Abrahams, S.C., and Keve, E.T. (1971) Normal probability plot analysis of error in measured and derived quantities and standard deviations. Acta Crystallographica, A27, 157–165.

Angel, R.J., Gasparik, T., Ross, N.L., Finger, L.W., Prewitt, C.T., and Hazen, R.M. (1988) A silica-rich sodium pyroxene phase with six-coordinated silicon. Nature, 335, 156–158.

Blessing, R.H. (1989) DREDD: Data reduction and error analysis for single crystal diffractometer data. Journal of Applied Crystallography, 22, 396–397.

Bolotovsky, R. (1994) Manual for IP software, p. 1–20. Chemistry Department, State University of New York, Buffalo, New York.

Bolotovsky, R., White, M.A., Darovsky, A., and Coppens, P. (1995) The "seed-skewness" method for integration of peaks on imaging plates. Journal of Applied Crystallography, 28, 86–95.

Brown, I.D. (1981) The bond-valence method: An empirical approach to chemical structure and bonding. In M.A. O'Keeffe and A. Navrotsky, Eds., Structure and bonding in crystals, vol. 2, p. 1–30. Academic, New York.

Brown, I.D., and Shannon, R.D. (1973) Empirical bond-strength–bond-length curves for oxides. Acta Crystallographica, A29, 266–282.

Calabrese, J.C. (1994) The computer program Z: On line help. DuPont, Wilmington, Delaware.

Finger, L.W., Ko, J., Hazen, R.M., Gasparik, T., Hemley, R.J., Prewitt, C.T., and Weidner, D.J. (1989) Crystal chemistry of phase B and an anhydrous analogue: Implications for water storage in the upper mantle. Nature, 341, 140–142.

Gasparik, T. (1989) Transformation of enstatite-diopside-jadeite pyroxenes to garnet. Contributions to Mineralogy and Petrology, 102, 389–405.

Gasparik, T., Wolf, K., and Smith, C.M. (1994) Experimental determination of phase relations in the $CaSiO_3$ system from 8 to 15 GPa. American Mineralogist, 79, 1219–1222.

Hazen, R.M., Downs, R.T., Finger, L.W., Conrad, P.G., and Gasparik, T. (1994) Crystal chemistry of Ca-bearing majorite. American Mineralogist, 79, 581–584.

Johnson, C.K. (1976) ORTEP: A Fortran thermal-ellipsoid plot program for crystal structure illustration. Oak Ridge National Laboratory, Oak Ridge, Tennessee.

Liebau, F. (1985) Structural chemistry of silicates, 347 p. Springer-Verlag, Berlin.

Pacalo, R.E.G., and Parise, J.B. (1992) Crystal structure of superhydrous B, a hydrous magnesium silicate synthesized at 1400 °C and 20 GPa. American Mineralogist, 77, 681–684.

Ringwood, A.E., and Major, A. (1971) Synthesis of majorite and other high pressure garnets and perovskites. Earth and Planetary Science Letters, 12, 411–418.

Sheldrick, G.M. (1986) SHELXS-86. Institut für Anorganische Chemie der Universität, Göttingen, Germany.

Swanson, D.K., and Prewitt, C.T. (1983) The crystal structure of $K_2Si^{VI}Si_3^{V}O_9$. American Mineralogist, 68, 581–585.

Manuscript received February 14, 1995
Manuscript accepted July 6, 1995